Ceramics International 43 (2017) 4212–4221

Contents lists available at ScienceDirect

Ceramics International

journal homepage: www.elsevier.com/locate/ceramint

Reactivity of $BaTiO_3$-$Ca_{10}(PO_4)_6(OH)_2$ phases in composite materials for biomedical applications

F.J. Vouilloz[a], M.S. Castro[a], G.E. Vargas[b], A. Gorustovich[b], M.A. Fanovich[a,*]

[a] Institute of Materials Science and Technology (INTEMA), University of Mar del Plata and National Research Council (CONICET), Av. J.B. Justo 4302, B7600FDQ Mar del Plata, Argentina

[b] Interdisciplinary Materials Group (IESIING-UCASAL, INTECIN UBA-CONICET), A4400EDD Salta, Argentina

ARTICLE INFO

Keywords:
Barium titanate
Hydroxyapatite
Biomedical composite
Solid state reaction

ABSTRACT

In this work the reactivity of barium titanate (BT) and hydroxyapatite (HA) composites from commercial and synthesized powders was studied. Raman spectroscopy, X-ray diffraction and scanning electron microscopy were used for characterization of sintered composites. Moreover, biotoxicity assays were performed to evaluate the effect of secondary phases in the sintered composites in relation to BT and HA phases. The formation of secondary phases and transformation of hydroxypatite into tricalcium phosphate depended on the reactivity of the starting materials. The piezoelectric voltage coefficient, calculed from permittivity and piezoelectric constant for composites containing 20 vol% HA, generated promising values for a good osteogenic response. The secondary phases formation during the sintering process favored the ions release to the incubation solution; consequently, the composite biocompatibility highly depended on samples composition. Composites made of synthesized HA and commercial BT produced valuable results for biomedical applications.

1. Introduction

The bone piezoelectric properties were reported by Fukada et al. in 1957 [1]. Bone tissue exhibits a very low piezoelectric coefficient of 0.7 pC/N [2] and responds to micromechanical stress such as body movement, leading to electrical dipole generation. These properties contributed to develop a new area of bone remodeling study. Consequently, new biomaterials with enhanced performance in bone regeneration can be designed considering these bone properties [3].

Hydroxyapatite ($Ca_{10}(PO_4)_6(OH)_2$, HA), a calcium phosphate with similar composition to that of the inorganic bone, can be polarized at 300–400 °C applying a 2 kV/cm electric field [4]. Bodhak et al. showed that the osseointegration rate can be modulated with the samples polarization degree. The possibility of producing piezoelectric composites between HA and lead-free traditional piezoelectric materials which could be suitable to apply in the human body has been explored. Barium titanate ($BaTiO_3$, BT) is the most frequently piezoelectric material used in bone replacement and repair, due to its excellent biocompatibility properties. Moreover, piezoelectric materials stimulate the implant attachment to the bone tissue, promoting bone regeneration [5,6]. Therefore, there is a great challenge in the development of HA-BT bioactive composite materials to improve the *in vivo* performance.

Feng et al. [7] showed that polarized HA-BT materials promote bone growth in higher degree than only HA depending on the direction of polarization. Hwang et al. [8] studied the effect of polarizing BT substrate in the formation of a calcium phosphate layer (CP) on the surface. They found out that the layer was formed on the CP negatively polarized side, whereas it was not observed on the positive side. In that study, three different polarization conditions were compared; however, the relation between piezoelectric properties and the CP layer formation was not studied. Bowen et al. [9] studied the influence of composition on dielectric properties of HA-BT composites finding that the incorporation of HA abruptly decreases dielectric permittivity (ε_r) and piezoelectric coefficient (d_{33}) values. They observed that samples with BT addition lower than 80% of BT did not show significant values of piezoelectric coefficient.

Several studies have shown that when a BT-HA bioceramic is polarized, a permanent residual charge on the surface is created, which can influence the response and activity of cells deposited on it [9,10]. However, some published works reported contradictory results related to the type of surface charge that improves the biological response [4].

In the preparation of dense BT-HA composites, the most important issue focuses on the reactivity of the crystalline BT and HA phases during the sintering process. This reactivity is detrimental for the reached piezoelectric properties after polarization because a high

* Corresponding author.
E-mail address: mafanovi@fi.mdp.edu.ar (M.A. Fanovich).

http://dx.doi.org/10.1016/j.ceramint.2016.12.053
Received 5 October 2016; Received in revised form 7 December 2016; Accepted 9 December 2016
Available online 10 December 2016

fraction of piezoelectric phases is missed after sintering. Dubey et al. [11] have reported the constituent HA and BT phases in HA-25 vol% BT and HA-35 vol% BT samples. However, they only showed X-ray diffraction patterns of HA-xBT samples before the spark plasma sintering. Baxter et al. [10] suggested the formation of secondary phases during the sintering process without clear experimental evidence.

This work aims at studying the reactivity of dense BT-20 vol% HA composites from commercial and synthesized powders of BT and HA, in order to evaluate the crystalline phases in the sintered materials. Raman spectroscopy, X-ray diffraction and scanning electron microscopy were used for characterization of sintered composites. Moreover, biotoxicity assays were performed to evaluate the effect of secondary phases in the sintered composites in relation to BT and HA phases. Additionally, the dielectric behavior on commercial BT and synthesized HA composites was analyzed considering the HA content.

2. Materials and methods

Commercial $BaTiO_3$ (cBT, Transelco Division, Ferro Corporation), commercial HA (cHA, Aldrich), synthesized $BaTiO_3$ (sBT) by mechanochemical method [12] and synthesized HA (sHA) by assisted precipitation process [13] were used as starting materials.

Approximately 6g of solid blend (80 vol% BT+20 vol% HA) were dispersed with isopropyl alcohol (10 mL) in a planetary mill (Fritsch Planetary Micro Mill Pulverisette 7) with zirconia balls (4 units) during 10 min at 890 rpm. Then, the blends were dried in an oven at 80 °C during 24 h. The obtained composite powders were used for sintering processing.

Three combinations were evaluated for reactivity: cBT/20 vol% cHA; sBT/20 vol% sHA and cBT/20 vol% sHA. Moreover, a series of cBT with 20, 40, 60 and 80 vol% sHA was prepared and dielectrically characterized.

Sintering processes were carried out on disc-shaped samples (12 mm diameter×1 mm thickness) in triplicate, prepared by the compactation of powder with PVA binder at 10 MPa using a hydraulic press. The compacted samples were then sintered in a Carbolite RHF 17/6 S in air at 1250 and 1300 °C for 1 h at a heating rate of 10 °C min^{-1}. Sintered samples were then ground using an agate mortar prior to characterization. The starting powders and the sintered samples were examined by X-ray diffraction (XRD) using a PANalytical, X'pert Pro diffractometer equipped with a Ni filtered CuKα radiation (λ=1.5406 Å).

Density values of the composites (ρ_S) were determined by the Archimedes' method using a Sartorius Balance (YDK01) with a density kit. Theoretical density (ρ_T) was calculated using Eq. (1).

$$\rho_T = (1 - V)\,\rho_{HA} + V\,\rho_{BT} \quad (1)$$

where ρ_{BT} is the BT theoretical density (5.61 g/cm^3), ρ_{HA} is the HA theoretical density (3.16 g/cm^3) and V is the initial filler volume fraction. The porosity (*P*) represents the "void space" of the sample and was calculated from % P=100 ($1-\rho_S/\rho_T$). Determinations were made in triplicate.

Thermogravimetric analysis and differential thermal analysis (TGA and DTA) of starting mechanical mixtures were performed employing a Shimadzu TGA-50 and DTA-50 under air atmosphere and using a 10 °C/min heating rate. In these assays, 20 mg of samples were employed.

Raman microspectrometric analyses of composites were performed on a multichannel Renishaw In Via Reflex microspectrometer. Excitation was provided by the 514 nm line of an Ar laser. To enhance the signal-to-noise ratio, 30–50 scans were accumulated, each one having a 15 s exposure to laser power ranging between 30 and 300 mW.

Morphologies of the samples were investigated by scanning electron microscopy (SEM), employing a Jeol 6460LV microscope after coating the samples with a thin gold layer. The obtained images were analyzed by means of the free access imaging software tool, ImageJ, to describe morphology and pore diameter of the studied materials. The composition of the ceramics was analyzed by x-ray Energy Dispersive Spectroscopy (EDS) characterizations, using an EDAX Genesis XM4 - Sys 60, equipped with Multichannel Analyzer EDAX mod EDAM IV.

Finally, samples were painted using silver paste and dielectric measurements were performed with a Hioki 3522-50 and a Hioki 3535 Impedance Analyzers from 1 Hz to 10 MHz. In order to test the piezoelectric coefficient, samples were polarized under a direct current (dc) electric field of 2160 V/mm in a silicone oil bath at 140 °C for 20 min. The piezoelectric constant d_{33} was measured using a piezo d_{33} meter (YE2730A d_{33} METER, APC International, Ltd., USA).

Biotoxicity assays were performed on dissolution products of milled sintered samples. For this test, embryonic zebrafish (*Danio rerio*) were used since they prove to be superior to conventional *in vivo* models. This test provides universal availability, relative low cost, rapid development and growth, and compliance with ethical rules for the use of experimental animals [14,15].

Powder of the samples was incubated in embryonic medium with a 1 wt% concentration (Hanks solution 10 wt%, pH=7) during 7 days in an orbital shaker at 37 °C to obtain the dissolution products. Then, the extracts were centrifuged and filtered with a 0.22 μm filter. In some extracts, it was necessary to adjust the pH to 7. Subsequently, dechorionated zebrafish embryos (48 h post fecundation) were incubated at 28.5 °C in plates during 72 h in an embryonic medium (control) or embryonic medium containing the dissolution products of each sample. The mortality rate was determined each 24 h between 0–72 h. To end the experiment, embryos were anesthetized with Tricaine and fixed in 4 wt% paraformaldehyde in Phosphate Buffered Saline (PBS). Assays were performed in duplicate with n=20 embryos for each sample. This assay determined the biocompatibility of the studied composite materials. The dissolution of Ba^{2+} from the incubated samples was quantified by X-ray fluorescence analysis (XRF, PW4025/24 Minipal2 X ray spectrometer Panalytical with a Cr tube anode).

3. Results and discussion

3.1. Characterization of synthesized and commercial powders

Fig. 1 shows the XRD patterns and the morphological feature of the starting materials. The diffraction patterns of commercial and synthetic barium titanate powders correspond to a perovskite structure (PDF#75-1169). Furthermore, synthesized powders present traces of $BaCO_3$ (PDF#1-0506) as a minority phase in the XRD pattern of Fig. 1a). The XRD pattern of cBT shows a doublet in the resolution of the signal at 2θ=45°, which is associated with the stabilization of the tetragonal BT phase.

The diffraction patterns of commercial and synthesized HA (Fig. 1b) show peaks corresponding to crystalline hydroxyapatite (PDF# 73-0294). Differences in the peaks' width and intensity can be attributed to different values of the crystallinity degree, crystal size and composition (different Ca/P molar ratio) of the samples.

Through scanning electron microscopy, the medium particle size and particle morphology were analyzed (Fig. 1). Particle size of synthesized BT (mean particle size lower than 10 nm) was smaller than that of the commercial BT (mean particle size of 0.9 μm).

Morphological features of used HA particles are completely different as it is shown in Fig. 1b. Commercial HA presents plate-like particles with 2.1 ± 0.4 μm thickness and a 40 μm side. On the other hand, synthesized HA particles present a rounded form because of the agglomeration of small particles. Therefore, agglomerates of 10–15 μm were formed due to the high superficial energy of nanoparticles.

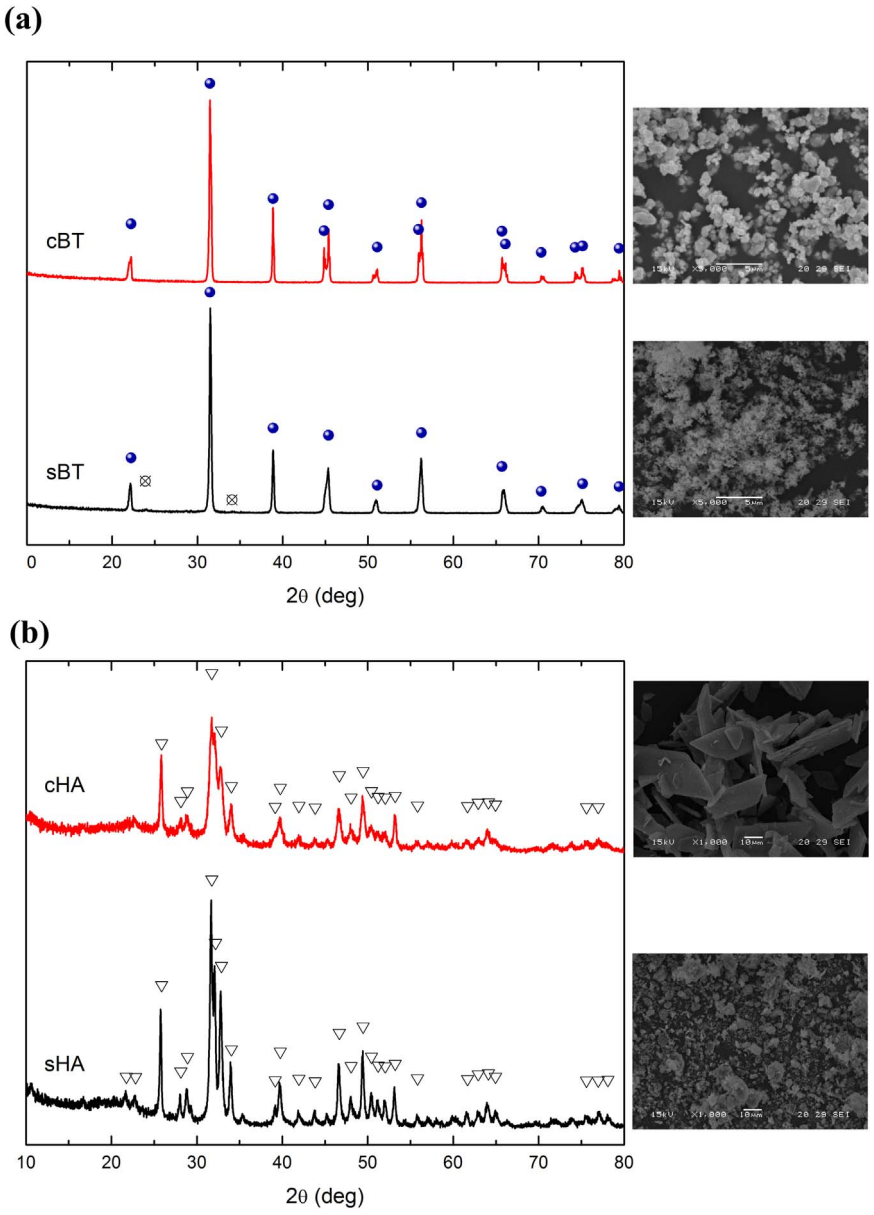

Fig. 1. X-Ray Diffraction patterns and SEM micrographs of: **a)** commercial (cBT) and synthetic (sBT) barium titanate; **b)** commercial (cHA) and synthetic (sHA) hydroxyapatite powders. ● BT (075-1169), ⊗ $BaCO_3$ (001-0506), ∇ HA (073-0294).

3.2. Sintering of composites from commercial powders (cBT-cHA)

Table 1 shows the density and porosity values of the samples sintered at 1250 °C and 1300 °C from commercial powders. From these results, a slight rise in the final density of pure materials with the increasing sintering temperature was registered. However, the effect of sintering temperature on composite samples did not improve the final density. Moreover, the final porosity augmented in 16% for a sintering temperature rising of 50 °C for sBT/20sHA composite. This effect can be due to the possible increasing reactivity between the original phases, resulting in a defective sintering process.

The final phase composition of sintered samples was evaluated from the XRD patterns shown in Fig. 2a and b. HA phase decomposition in cHA and cBT-20cHA composite is observed in Fig. 2. BT peaks were moved to higher 2θ values due to Ba^{2+} substitution by Ca^{2+} in the perovskite structure. Moreover, typical diffraction signals of secondary phases like barium phosphate, Ba3(PO4)2 (PDF# 25-0028), and barium calcium phosphate, Ba2,1Ca0,9(PO4)2 (PDF# 24-0092), were observed. Thermally treated BT powders displayed the characteristic

Table 1
Density, theoretical density and porosity values of sintered samples. Results were obtained from three samples of each composition.

	Material	Density (g/cm^3)	Theoretical density (g/cm^3)	Porosity (%)
1250 °C	cHA	2.83 ± 0.06	3.15	10.1 ± 2.0
	cBT/20cHA	5.18 ± 0.08	5.44[a]	4.7 ± 1.5
	cBT	5.75 ± 0.10	6.02	4.6 ± 1.7
	sBT/20sHA	4.84 ± 0.12	5.44[a]	11.0 ± 2.2
1300 °C	cHA	2.87 ± 0.03	3.15	8.9 ± 1.0
	cBT/20cHA	5.17 ± 0.10	5.44[a]	5.0 ± 1.8
	cBT	5.81 ± 0.04	6.02	3.5 ± 0.7
	sBT/20sHA	4.74 ± 0.09	5.44[a]	12.8 ± 1.7

[a] Theoretical density was calculated assuming that the final composites are formed by HA and BT pure phases.

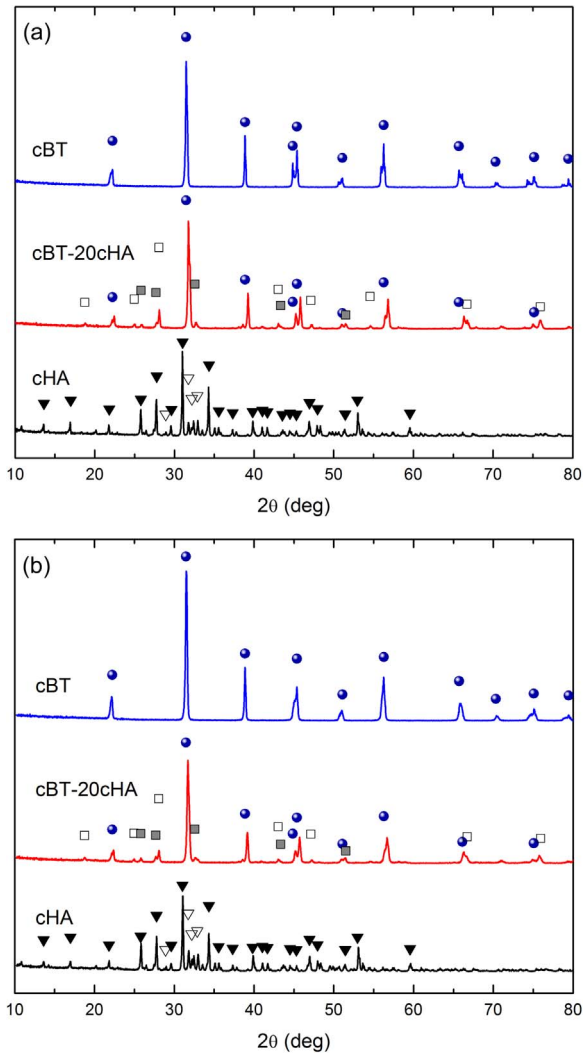

Fig. 2. X-Ray Diffraction patterns of samples sintered at **(a)** 1250 °C and **(b)** 1300 °C from commercial BT, commercial HA and cBT-20cHA powders. ● BT (075-1169), □ $Ba_3(PO_4)_2$ (025-0028), ■ $Ba_{2.1}Ca_{0.9}(PO_4)_2$ (24-0092), ▼ β-TCP (070-2065), ∇ HA (073-0294).

split associated with the tetragonal symmetry of the perovskite phase between 2θ 44 and 47° [16]. This split was amplified when the sintering temperature increased from 1250 to 1300 °C. Taking into account that samples sintered at 1300 °C presented a higher tetragonal level than samples sintered at 1250 °C, and that tetragonal perovskite structure displayed ferroelectric and piezoelectric behavior, 1300 °C was the selected temperature for the sintering process.

Composites sintered at 1300 °C were examined through Raman spectroscopy (Fig. 3). Spectra show a sharp band at 305 cm^{-1} [B1, E(TO+LO)] and wide bands at 248 cm^{-1}, 519 cm^{-1} and 713 cm^{-1} corresponding to [A1(TO)], [A1, E(TO)] and [A1,E(LO)] vibration modes associated with tetragonal barium titanate [17,18]. The existence of this phase agrees with the split observed through XRD at 2θ=44–47°. The typical HA Raman spectrum is dominated by the ν_1 stretching mode of the P-O vibration at 961 cm^{-1} as a single intense peak, whereas those two peaks and a shoulder can be observed in the β-TCP phase [19]. Fig. 3 clearly exhibits the β-TCP phase in the cHA sample, sintered at 1300 °C, in agreement with the structure detected through XRD analysis. Characteristic bands of the HA phase were not detected in cBT/20cHA composites due to HA decomposition in the mixture producing secondary phases and substituted titanates.

Micrographs of composite ceramics are shown in Fig. 4. Because of changes in the composition, differences in the average grain size and

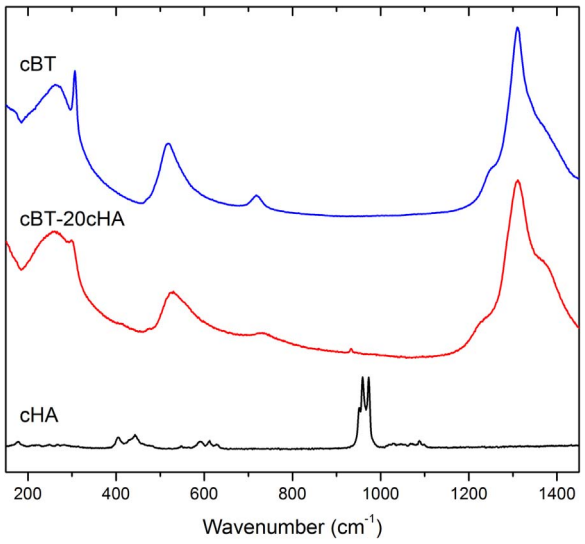

Fig. 3. Raman spectra of samples sintered at 1300 °C from commercial BT, commercial HA and cBT-20cHA powders.

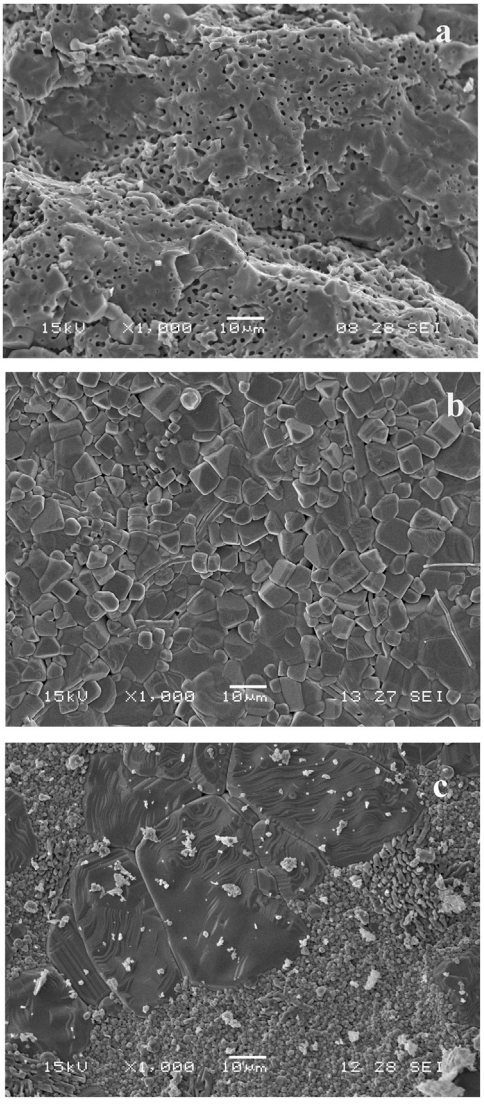

Fig. 4. Microstructures of samples sintered at 1300 °C: **a)** commercial HA; **b)** cBT/20cHA; **c)** commercial BT powders.

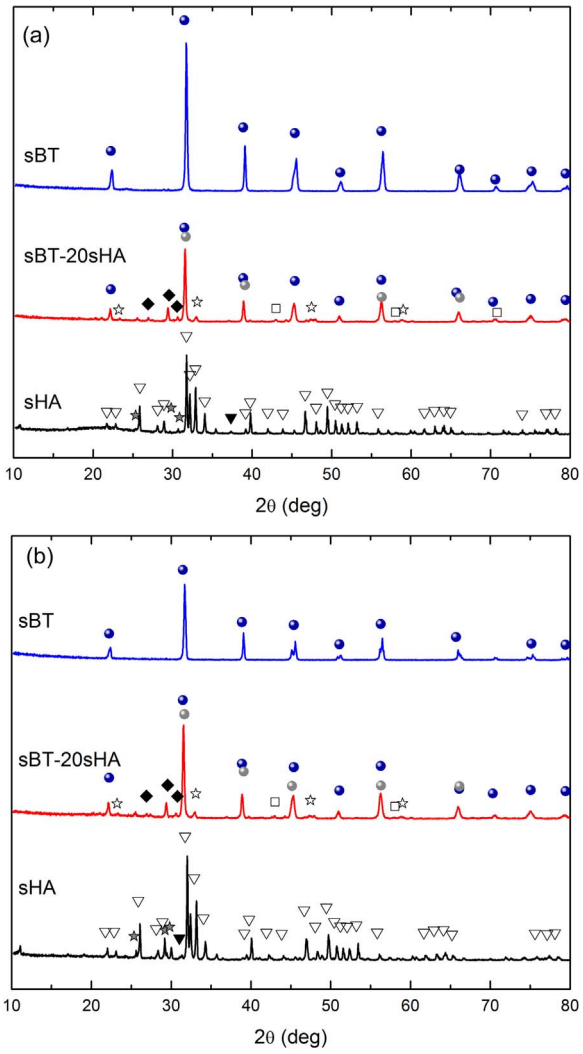

Fig. 5. X-Ray Diffraction patterns of samples sintered at **(a)** 1250 °C and **(b)** 1300 °C from synthesized BT, synthesized HA and sBT-20sHA powders. ● BT (075-1169), ● $(Ba_{0.88}Ca_{0.12})TiO_3$ (081-1288), ☆ $CaTiO_3$ (076-2400), ◆ $Ca_2P_2O_7$ (020-0024), □ $Ba_3(PO_4)_2$ (025-0028), ★ TTCP (025-1137), ▼ β-TCP (070-2065), ▽ HA (073-0294).

morphology were detected in the fracture surface of the sintered materials. The pure cHA samples microstructure resulted to be highly porous with a medium pore size of 0.85 μm, whereas, BT samples displayed a bimodal grain size distribution (grains of 35 μm and 0.5–2 μm). In cBT/20cHA samples, a homogeneous microstructure with a medium grain size of 8 μm and the formation of barium phosphate as secondary phases were observed.

These results confirm that HA and BT commercial phases react during sintering process producing secondary phases and lowering the hydroxyapatite amount in the final composites.

3.3. Sintering of composites from synthesized powders (sHA-sBT)

Fig. 5 shows the XRD patterns of thermally treated synthesized powders at 1250 °C (Fig. 5a) and 1300 °C (Fig. 5b). Peaks associated with barium titanate were observed in sBT samples sintered at 1250 °C or 1300 °C. Slight differences between samples sintered at 1250 °C or 1300 °C were detected. Contrary to that observed for samples prepared from commercial powders, the characteristic split of the tetragonal phase at 2θ=45° was only observed in sBT samples at 1300 °C. sHA samples sintered at 1250 °C or 1300 °C presented characteristic peaks of the hydroxyapatite phase and others, of lower intensity, associated with secondary phases (tricalcium phosphate, β-TCP PDF# 70–2065,

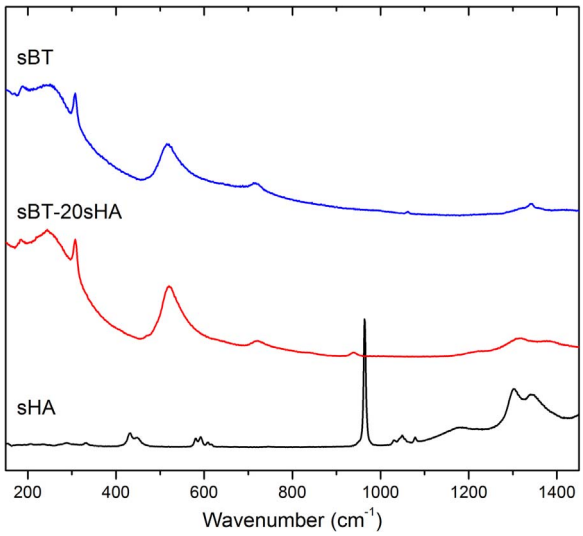

Fig. 6. Raman spectra of samples sintered at 1300 °C from synthesized BT, synthesized HA powders and sBT-20sHA powders.

and tetracalcium phosphate, TTCP, Ca4O(PO4)2, PDF# 25-1137).

The sBT/20sHA composites showed peaks assigned to barium titanate perovskite and secondary phases as calcium titanate (CaTiO3, PDF# 76-2400), barium calcium titanate ((Ba0.88Ca0.12) TiO3, PDF# 81-1288), calcium pyrophosphate ($Ca_2P_2O_7$, PDF# 20–0024) and traces of barium phosphate ($Ba_3(PO_4)_2$, PDF# 25-0028).

Bands at 303, 519 y 713 cm^{-1} associated with tetragonal barium titanate were observed through Raman spectroscopy in sBT and sBT/20sHA samples (Fig. 6). These signals indicated that the tetragonal structure of BT was stabilized in samples sintered at 1300 °C. Typical bands of HA were not observed in sBT/20sHA composites indicating that the hydroxyapatite phase reacted with barium titanate producing substituted barium titanates and secondary phases.

As regards the densification process, sBT/20sHA samples sintered at 1250 °C and 1300 °C presented lower density values than composites obtained from commercial powders (Table 1).

Taking into account the lowest reactivity of synthesized hydroxyapatite and the highest tetragonal degree of commercial barium titanate, a new series of composites was formulated from commercial BT and synthesized HA powders.

3.4. Sintering of composites from commercial BT and synthesized HA powders (cBT-sHA)

Considering the above results and in order to increase the tetragonal ratio of composites, sintering temperature was fixed at 1300 °C. Fig. 7 shows the crystalline phases detected through XRD in composites sintered at 1300 °C, the series contains a gradual amount of nominal HA from 0 to 100 vol%. From XRD patterns, a reduction in the tetragonal signal of BT with the HA increasing amount in the composites was observed. The peak at 2θ=45° becomes wider in cBT/20sHA sample due to the coexistence of both cubic and tetragonal phases of barium titanate. Calcium titanate ($CaTiO_3$) and barium phosphate ($Ba_3(PO_4)_2$ crystalline phases were stabilized in cBT/20sHA and cBT/40sHA samples.

Fig. 8 shows the thermal behavior of starting mechanical mixtures of the cBT and sHA series with 20, 40, 60 and 80 vol% of HA. The mass loss is associated with the HA amount in the mixture. This mass loss is attributed to the adsorbed and lattice water (between 20 and 600 °C); the CO_2 loss from carbonated HA (between 600 and 1000 °C) and dehydroxylation of HA to produce oxihydroxyapatite ($Ca_{10}(PO_4)_6(OH)_{2-2x}$ $O_x\square_x$) and H_2O(g) (between 1000 and 1400 °C) [20]. The higher HA content in the mixture, the greater the mass loss.

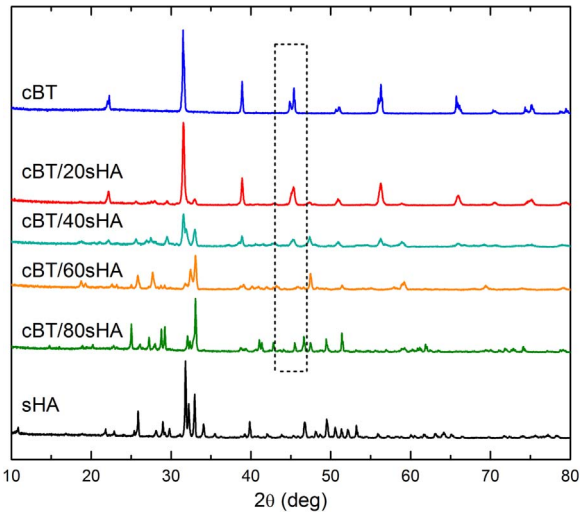

Fig. 7. X-Ray Diffraction patterns of composites sintered at 1300 °C from commercial BT and synthesized HA powders.

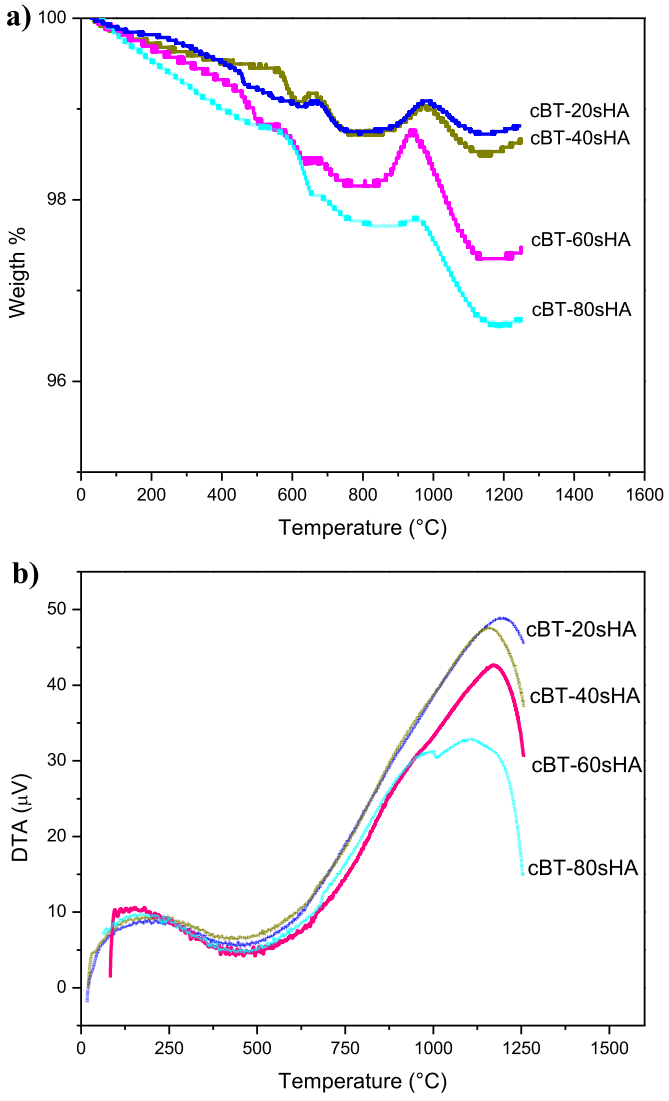

Fig. 8. a) Termogravimetric Analysis (TGA) and **b)** Differential Thermal Analysis (DTA) of starting mechanical mixtures between cBT and sHA.

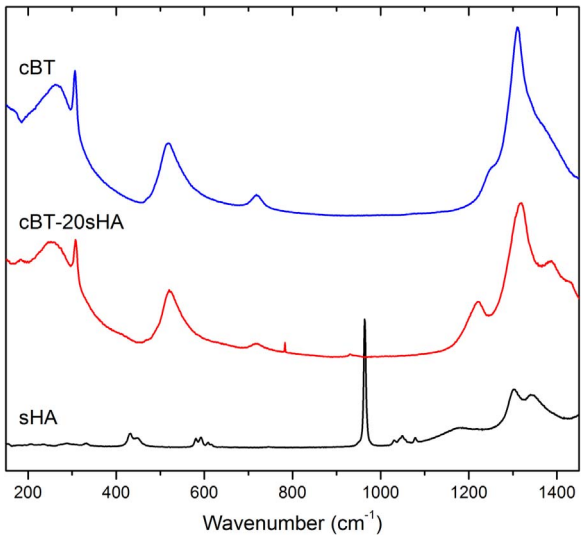

Fig. 9. Raman spectra of samples sintered at 1300 °C from commercial BT, synthesized HA and cBT-20sHA powders.

In all cases the mass loss does not exceed 4% in weight (Fig. 8a). DTA curves suggest that the heat treatment enables the formation of liquid phase from 1150 °C. This liquid phase, produced by the partial dissolution of the phosphates and titanates phases, allows the crystallization of secondary phases during the cooling process because HA thermodynamic stability strongly depends on the water pressure of the environment. The presence of HA in the sintered samples would come from the decomposition of non-stoichiometric HA and would not come from of the liquid phase formed at high temperature. However, as it is observed in XRD spectra (Fig. 7), HA phase is not detected, specially, in cBT-80sHA and cBT-60sHA, whereas a crystalline HA phase would be expected in non-reactive system.

The characteristic bands of tetragonal BT at 303, 519 and 713 cm^{-1} were observed through Raman spectroscopy in cBT/20sHA (Fig. 9). This observation confirms the tetragonal phase stabilization in the sample containing nominal 20 vol% of HA. However, no signals of HA existence were detected due to HA decomposition and the secondary phases formation.

Fig. 10 shows the microstructures of fractured surfaces of sintered composites at 1300 °C from cBT containing different amounts of nominal sHA. The barium titanate sample (Fig. 10a) exhibits a bimodal grain size distribution with 2 μm and 20–30 μm grains.

cBT/20sHA (Fig. 10b) and cBT/40sHA (Fig. 10c) samples developed a dense microstructure with homogeneous grain size and small pore size. In cBT/60sHA (Fig. 10d) and cBT/80sHA (Fig. 10e) samples, micro and macropores were produced associated with hydroxyapatite decomposition and liquid formation at the sintering temperature. The HA sample shows a porous microstructure (Fig. 10f) with uniform grain size of 2–3 μm of mean diameter.

Table 2 shows the measured density and the calculated porosity for each composite of the cBT and sHA series. The porosity degree decreased as the BT increasing in the composites, except for the cBT/60sHA sample that registers 36% porosity. This unusual behavior can be assigned to the secondary phases generated by reaction between the BT and HA original phases. In the cBT/60sHA sample, similar phases of $BaTiO_3$ and $CaTiO_3$ were identified along with $Ca_2P_2O_7$ through XRD (Fig. 7).

Formation of secondary phases during the sintering process of barium titanate and hydroxyapatite was also suggested by Baxter et al. [10]. However, the authors did not identify secondary phases through XRD. The formation of β-tricalcium phosphate, barium phosphate, calcium barium hydrogen phosphate and barium titanium phosphate was only suggested. Few studies in literature consider the possible

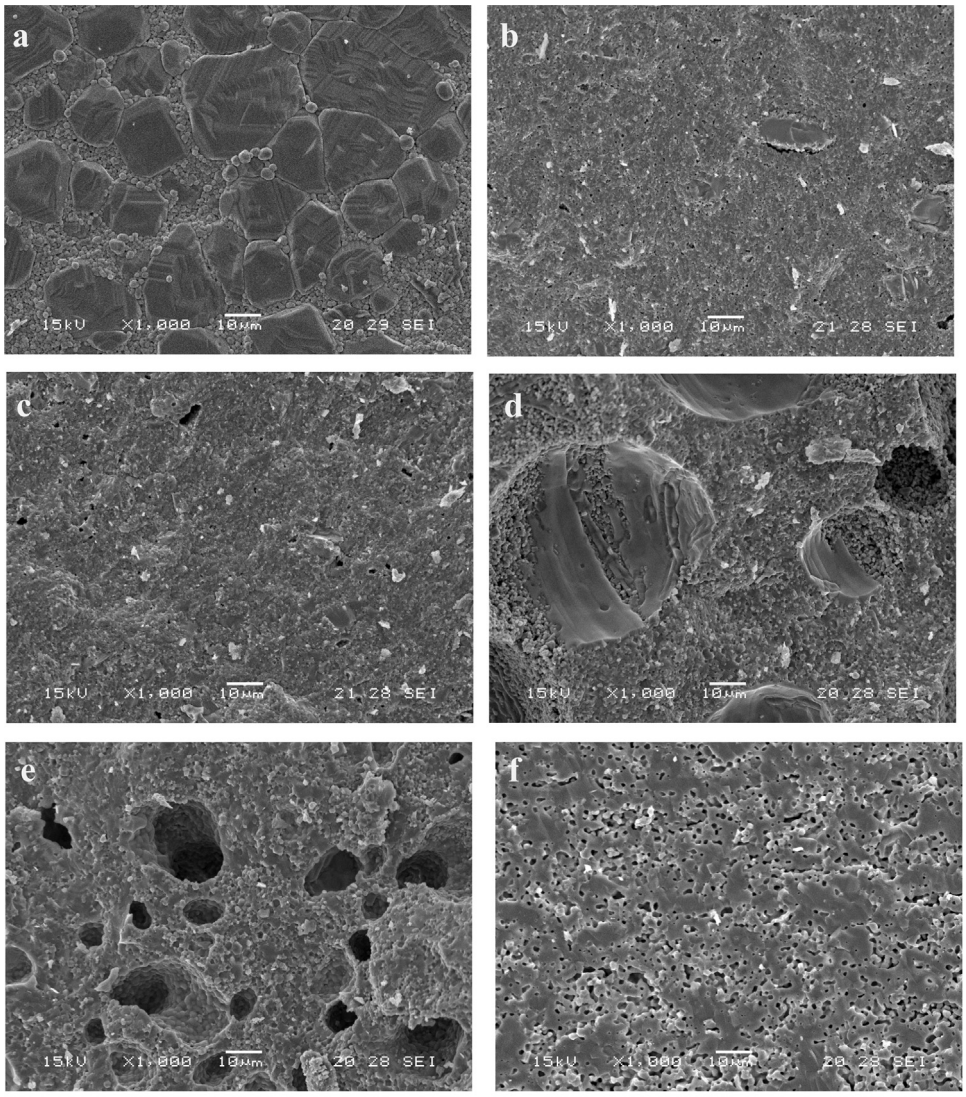

Fig. 10. SEM micrographs of samples sintered at 1300 °C: **a)** cBT; **b)** cBT/20sHA; **c)** cBT/40sHA; **d)** cBT/60sHA; **e)** cBT/80sHA; **f)** sHA.

Table 2
Density, theoretical density and porosity values of sintered samples at 1300 °C from commercial BT and synthesized HA powders. Results were obtained from three samples of each composition.

Material	Density (g/cm^3)	Theoretical density (g/cm^3)	Porosity (%)
sHA	2.60 ± 0.04	3.15	17.4 ± 1.3
cBT/80sHA	3.07 ± 0.14	3.72[a]	17 ± 4
cBT/60sHA	2.74 ± 0.05	4.30[a]	36.3 ± 1.2
cBT/40sHA	4.46 ± 0.09	4.87[a]	8.4 ± 1.8
cBT/20sHA	5.09 ± 0.05	5.44[a]	6.5 ± 1.0
cBT	5.81 ± 0.04	6.02	3.5 ± 0.7

[a] Theoretical density was calculated assuming that the final composites are formed by HA and BT pure phases.

reaction between $BaTiO_3$ and hydroxyapatite. In those studies, all composite samples reacted during the sintering process in greater or lesser proportion, according to the thermal stability of the crystalline phases. A recent publication [11] reported the preparation of porous samples with varying amounts of BT in HA by using spark plasma sintering. These authors discuss the composition of phases before the sintering process but without explaining the stabilized phases after the sintering treatment. The authors analyze the dielectric behavior but do not contribute directly to the study of piezoelectric or cytotoxic performance.

Dielectric and piezoelectric behavior of sintered composites can be described with the evaluation of dielectric permittivity (ε_r) and piezoelectric coefficient (d_{33}) values. These parameters can be related to microstructure features, crystalline phases distribution and the densification degree. Fig. 11 shows the dielectric permittivity of the composites in sintered samples at 1300 °C. As it was expected [21], dielectric permittivity values increased with barium titanate concentration. Samples of pure BT exhibit lower values (aprox. to 170 at 20 kHz) than the ones reported in literature (between 2000 and 4500) [22,23]. This difference can be attributed to microstructure characteristics of sintered samples such as remnant pores and the high amount of small grains, with low tetragonal degree. The composite samples exhibited similar dielectric permittivity values than those reported in literature for mixed composites [23], while higher values than the ones prepared in two layers' geometry using the screen printing technique were obtained [21].

Experimental real permittivity values were fitted with the rule of mixtures, using Eq. (2) for parallel and series configuration as follows,

$$\varepsilon_c^n = f_{BT} \cdot \varepsilon_{BT}^n + f_{HA} \cdot \varepsilon_{HA}^n, \quad (2)$$

where, n equals 1 for a parallel configuration, and −1 for a series configuration, f_{BT} and f_{HA} are the barium titanate and hydroxyapatite volume fraction, respectively [24].

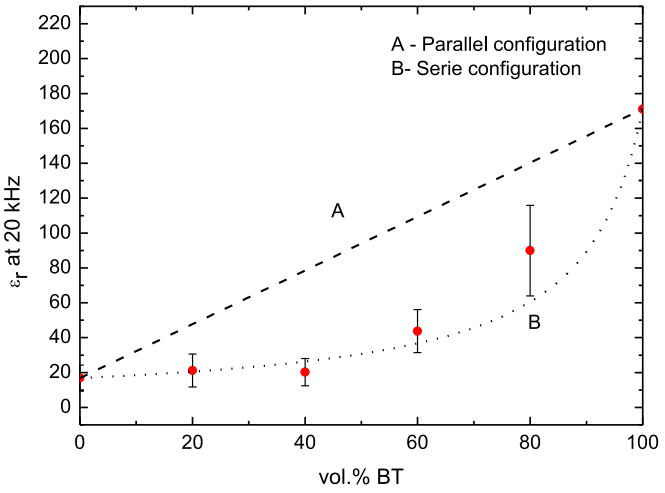

Fig. 11. Dielectric permittivity (ε_r) of cBT/sHA series vs. vol% BT.

Experimental data can be fitted with the series configuration, indicating that phases were well mixed and parallel preferential form was not displayed in the sintered samples. Moreover, formation of secondary phases, residual porosity and wide grain size distribution could contribute to deviations from the theoretical models. Bowen et al. also observed similar behavior in the relative permittivity as a function of $BaTiO_3$ content [9].

The piezoelectric constant measured on sintered and polarized cBT was d_{33}=37 ± 16 pC/N, while that for the cBT/20sHA sample was d_{33}=13 ± 3 pC/N. For the HA-$BaTiO_3$ composites the addition of a non-piezoelectric HA ceramic leads to an increased level of matrix 'clamping', which could account for the rapid decrease in d_{33} [23]. On the other hand, the high porosity level showed in samples with low barium titanate concentration impeded the polarization process using the direct current arrangement, whereby the piezoelectric constant was not determined in cBT/40sHA, cBT/60sHA and cBT/80sHA samples.

The measured d_{33} values were higher than the natural bone ones (0.7 pC/N) [2]. Zhang *et al.* [25] obtained a d_{33} value of 2.8 pC/N for a porous composite with 10 vol% HA which resulted comparable to Bowen's result with a d_{33} value ~4 pC/N [9], which was based on a 10 wt%HA composite bulk. Bowen's later report indicated an improved d_{33} value of ~70 pC/N [9] for the 10 vol%HA composite and a value close to 20 pC/N for a 20 vol%HA composite [23] although the experimental procedures in both reports were similar. Moreover, Gittings et al. determined that at least 80% volume of $BaTiO_3$ is needed for the composites to exhibit stress-induced piezoelectric potential [23]. In this study, the obtained piezoelectric constant values, for the system formed with commercial BT and synthesized HA, were similar to those reported in literature.

Additionally, permittivity and d_{33} helped to estimate the field developed by calculation of the piezoelectric voltage coefficient, g_{33} ($g_{33}=d_{33}/\varepsilon_{composite}$). Although the g_{33} coefficient decreases from approximately 24.58×10^{-3} V m^{-1} Pa^{-1} for 100% $BaTiO_3$ to 17.27×10^{-3} V m^{-1} Pa^{-1} for composites containing 20 vol% HA, calculated values are higher than those obtained by Bowen et al. [9]. Moreover, considering a stress of 0.1 MPa applied to a cBT/20sHA composite of 100 μm thickness, a potential of 0.173 V is generated, a value similar to that reported by Marino et al. [26] on piezoelectric polyvinylidene fluoride and by Sapadaro [27] which were shown to enhance bone formation. Thus, the piezoelectrically induced voltage reported here is comparable in magnitude to the electrochemically generated voltages associated with osteogenic responses in other biological studies.

Taking into account the stabilized phases, final microstructure, and dielectric and piezoelectric properties, cBT/20sHA composites generated promising values for a good biological response.

Table 3
Cytotoxical assays: influence of the composition on the biological response.

Sample	Ba^{2+} (ppm)	% Mortality			
		24 h	48 h	72 h	Total
Control	0	0	0	0	0
sHA	0	0	0	0	0
cHA	0	0	0	0	0
sBT	537	0	0	100	100
cBT	0	0	0	0	0
cBT/20cHA	582	0	0	100	100
cBT/20sHA	244	0	0	0	0
sBT/20sHA	826	0	0	100	100

3.5. Biotoxicity and thermal behavior of BT-20HA composites

From the above results, it is possible to conclude that a high HA content was detrimental for the stabilization of the ferroelectric structure (tetragonal phase) in sintered composites. Therefore, biotoxicity assays were performed only on BT-20HA series and on starting materials.

In order to find the influence of the composition on the biological response, their biotoxicity were assessed in zebrafish embryos. For more than 60 years, zebrafish have been used in toxicological studies. They combine some of the high-throughput and molecular biology advantages of *in vitro* systems (e.g. cell culture) but add the relevance of whole-organism *in vivo* studies [14]. Table 3 shows the obtained results.

BT has also been reported to be a potential bioactive material. It could induce apatite formation in simulated body fluid, and it could enhance bone formation in a biological environment because of its piezoelectric properties [28]. However, the sBT synthesized from $BaCO_3$ and TiO_2 showed toxical behavior after 72 h of incubation time, making a substantial difference for the commercial BT that did not show biotoxic effects. This fact can be associated with an incomplete conversion of the reaction during the synthesis process, expelling Ba^{2+} ions to the solution where embryos incubation proceeds.

On the other hand, materials with a composition based on calcium phosphate have a recognized biocompatibility. In the assayed HA materials, both showed the expected behavior.

Interesting behavior resulted from the cBT/20sHA sample in contrast with the other analyzed composites. The composite formed by commercial BT and 20 vol% synthesized HA did not show a cytotoxic effect, while the rest of the analyzed composites showed a cytotoxic effect after 72 h of incubation. In fact, there is a direct correlation between the samples that contain secondary phases (detected by XRD), the lixiviated Ba^{2+} ions and their cytotoxicity. To fully understand this behavior, crystalline stabilized phases must be considered.

Fig. 12 shows the thermal behavior of the starting mixtures of sBT-20sHA, sBT-20cHA and cBT-20sHA (TGA and DTA curves). The three studied mixtures presented a similar behavior with the typical mass loss as a function of temperature as that previously described for the cBT-sHA series. Moreover, it can be observed in Fig. 12b that cBT-20sHA sample shows lower trend to form a liquid phase during the sintering process than sBT-20sHA, sBT-20cHA samples.

Taking into account the evolution of the mixture with the temperature and the crystalline phases detected in the sintered composites, the following unbalanced reactions are proposed for each studied mixture:

Sample cBT/20cHA

$Ca_{10-x}(PO_4)_{6-x}(HPO_4)_x(OH)_{2-x}+BaTiO_3\rightarrow$
$Ba_3(PO_4)_2+Ba_{2.1}Ca_{0.9}(PO_4)_2+H_2O+Ba_{0.88}Ca_{0.12}TiO_3$.

0 < x < 1 Non stoichiometric

Sample sBT/20sHA

$Ca_{10}(PO_4)_6(OH)_2+BaTiO_3\rightarrow Ca_2P_2O_7+CaTiO_3+H_2O$

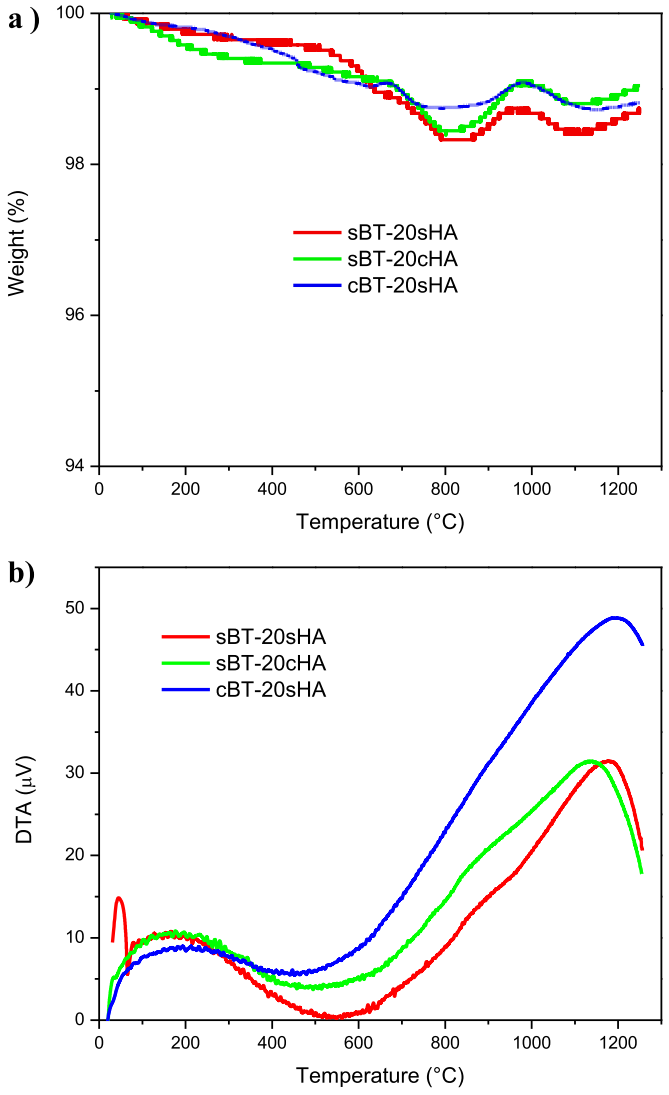

Fig. 12. a) Termogravimetric Analysis (TGA) and **b)** Differential Thermal Analysis (DTA) of starting mechanical mixtures: sBT-20sHA, sBT-20cHA and cBT-20sHA.

$+Ba_{0.88}Ca_{0.12}TiO_3+Ba_3(PO_4)_2$

Stoichiometric

Sample cBT/20sHA

$Ca_{10}(PO_4)_6(OH)_2+BaTiO_3 \rightarrow H_2O$

$+Ba_{0.88}Ca_{0.12}TiO_3+CaTiO_3+Ca_3(PO_4)_2$

Stoichiometric

During the sintering process, cBT/20cHA sample decomposes to produce tetragonal barium titanate with a partial substitution of barium by calcium and a small number of secondary phases. The non-stoichiometric cHA phase results reactive with cBT giving place to the formation of soluble phases as $Ba_3(PO_4)_2$. The produced secondary phase dissolves in the culture medium reducing the viability. Conversely, for composite samples from synthetic powders, the hydroxyapatite phase was stable restricting the ions substitution. However, in this case the synthetic barium titanate resulted a reactive phase facilitating the sHA desproportion (deshydroxylation) and favoring the formation of calcium-rich secondary phases ($Ca_2P_2O_7$; $CaTiO_3$) and traces of $Ba_3(PO_4)_2$.

Finally, composites from commercial barium titanate and 20 vol% synthetic hydroxyapatite were thermally stable with a low amount of non-soluble secondary phases as $CaTiO_3$ and $Ca_3(PO_4)_2$. Consequently, stable phases can be associated with a low solubility level which inhibits ions release in the culture medium and favors the sample biocompatibility. This study demonstrates that reactivity between the precursor phases of the composites impairs their performance as biomaterial. In these systems, cytotoxicity may fall on the great dissolution of Ba^{2+} ions which presumably come from $Ba_3(PO_4)_2$ secondary phase. The observed biotoxic behavior is in accordance with the quantified Ba^{2+} ions in solution after incubation of each sintered samples (see Table 3).

To sum up, BT-HA composites for possible biomedical applications must verify the following features:

- High tetragonal/cubic ratio for BT phase. A sintering temperature of 1300 °C improves this ratio. Analyzing the signal at 44–46° by XRD it is possible to determine the stabilized tetragonal structure.
- Reduced reactivity between BT and HA at the sintering temperature. The reactivity only can be reduced if a limited stoichiometric HA amount is present in the mixture (20 vol% HA in this study). Large amounts of stoichiometric HA or even non-stoichiometric HA induce reactivity promoting liquid phase formation. During the cooling process $Ba_3(PO_4)_2$ crystallizes as a secondary phase. This barium phosphate favors the Ba^{2+} ions lixiviation into the culture medium increasing the biotoxicity.
- Suitable percentage of porosity. A balance between polarization and sample porosity must be considered. In this type of biomaterials osteoconduction properties are favored when a porous microstructure is formed. Large amounts of HA favor the liquid phase formation and consequently, a porous microstructure is developed. Nevertheless, polarization is improved when porosity is reduced, and when a high tetragonality level is stabilized. Finally, as the HA content increases the polarization process is obstructed.

Taking into account the mentioned features for the BT - HA composites, the cBT-20sHA sample registered the lowest biotoxicity level related to the formation of stable secondary phases ($CaTiO_3$ and $Ca_3(PO_4)_2$) and a high piezoelectric voltage coefficient (17.27×10^{-3} V m^{-1} Pa^{-1}).

4. Conclusions

From the experimental results, it is possible to conclude that stability of the starting materials was crucial for system reactivity. Although, there are no concluding reports about possible reactivity between starting materials, in this work the formation of secondary phases in the sintering process was identified by XRD, contributing to the knowledge of these composites. Moreover, thermal stability differences between commercial and synthesized materials were observed. The formation of secondary phases and transformation of hydroxypatite into tricalcium phosphate depended on the reactivity of the starting materials. Composites made of synthesized HA and commercial BT produced promising results for biomedical applications. The piezoelectrically induced voltage calculed from permittivity and piezoelectric constant for composites containing 20 vol% HA resulted promising values for a good osteogenic response. Even though density of composite samples increased with barium addition, samples with 80 or 60 vol% HA showed high porosity levels due to the formation of secondary phases. The secondary phases formation during the sintering process favored the ions release to the incubation solution, consequently the composite biocompatibility highly depended on samples composition.

Acknowledgements

The authors thank the following institutions for providing financial support: National Research Council (CONICET, Argentina) Project PIP 1851, University of Mar del Plata (Argentina) Project (15G/388).

References

[1] E. Fukada, I. Yasuda, On the piezoelectric effect of bone, J. Phys. Soc. Jpn. 12 (1957) 1158–1162.
[2] A. Bur, Measurements of the dynamic piezoelectric properties of bone as a function of temperature and humidity, J. Biomech. 1 (1976) 495–507.
[3] Y. Zhang, L. Chen, J. Zeng, K. Zhou, D. Zhang, Aligned porous barium titanate/hydroxyapatite composites with high piezoelectric coefficients for bone tissue engineering, Mater. Sci. Eng.: C 39 (2014) 143–149.
[4] S. Bodhak, S. Bose, A. Bandyopadhyay, Role of surface charge and wettability on early stage mineralization and bone cell–materials interactions of polarized hydroxyapatite, Acta Biomater. 5 (2009) 2178–2188.
[5] J.B. Park, S.D. Brown, J.K. Scott, Mechanical property changes of barium titanate (ceramic) after in vivo and in vitro aging, *Biomater*., Med. Devices Artif. Organs 5 (1977) 267–276.
[6] J.B. Park, B.J. Kelly, G.H. Kenner, A.F. von Recum, M.F. Grether, Piezoelectric ceramic implants: in vivo results, J. Biomed. Mater. Res. Part A 15 (1981) 103–110.
[7] J.Q. Feng, H.P. Yuan, X.D. Zhang, Promotion of osteogenesis by a piezoelectric biological ceramic, Biomaterials 18 (1997) 1531–1534.
[8] K.S. Hwang, J.E. Song, J.W. Jo, H.S. Yang, Y.J. Park, J.L. Ong, H.R. Rawls, Effect of poling conditions on growth of calcium phosphate crystal in ferroelectric $BaTiO_3$ ceramics, J. Mater. Sci.: Mater. Med. 13 (2002) 133–138.
[9] C.R. Bowen, J. Gittings, I.G. Turner, F. Baxter, J.B. Chaudhuri, Dielectric and piezoelectric properties of hydroxyapatite-$BaTiO_3$ composites, Appl. Phys. Lett. 89 (2006) 132906.
[10] F.R. Baxter, I.G. Turner, C.R. Bowen, J.P. Gittings, J.B. Chaudhuri, An in Vitro Study of Electrically Active Hydroxyapatite-Barium Titanate Ceramics using Saos-2 Cells, J. Mater. Sci.: Mater. Med. 20 (2009) 1697–1708.
[11] A.K. Dubey, K. Kakimoto, Impedance spectroscopy and mechanical response of porous nanophase Hydroxyapatite-Barium Titanate composite, Mater. Sci. Eng.: C C 63 (2016) 211–221.
[12] E. Brzozowski, M.S. Castro, Lowering the synthesis temperature of high-purity $BaTiO_3$ powders by modifications in the processing conditions, Thermochim. Acta 398 (1–2) (2003) 123–131.
[13] M.A. Giardina, M.A. Fanovich, Synthesis of nanocrystalline hydroxyapatite from $Ca(OH)_2$ and H_3PO_4 assisted by ultrasonic irradiation, Ceram. Int. 36 (2010) 1961–1969.
[14] J.T. Gamse, D.A. Gorelick, Mixtures, metabolites, and mechanisms: understanding toxicology using zefrafish, Zebrafish 13 (2016) 377–378.
[15] V.E. Fako, D.Y. Furgeson, Assessing biomaterial nanotoxicity with a novel zebrafish model, Adv. Drug Deliv. Rev. 61 (2009) 478–486.
[16] E. Brzozowski, A.C. Caballero, M. Villegas, M.S. Castro, J.F. Fernández, Effect of doping method on microstructural and defect profile of Sb-$BaTiO_3$, J. Eur. Ceram. Soc. 26 (12) (2006) 2327–2336.
[17] L.H. Robins, D.L. Kaiser, L.D. Rotter, P.K. Schenck, G.T. Stauf, D. Rytz, Investigation of the structure of barium titanate thin films by Raman spectroscopy, J. Appl. Phys. 76 (1994) 7487–7498.
[18] H.A. Avila, L.A. Ramajo, M.M. Reboredo, M.S. Castro, R. Parra, Hydrothermal synthesis of $BaTiO_3$ from different Ti-precursors and microstructural and electrical properties of sintered samples with submicrometric grain size, Ceram. Int. 37 (7) (2011) 2383–2390.
[19] R. Cuscó, F. Guitián, S. de Aza, L. Artús, Differentiation between hydroxyapatite and β-Tricalcium phosphate by means of μ-Raman Spectroscopy, J. Eur. Ceram. Soc. 18 (1998) 1301–1305.
[20] M.A. Fanovich, J.M. Porto López, Influence of temperature and additives on the microstructure and sintering behavior of hydroxyapatites with different Ca/P ratio, J. Mater. Sci.: Mater. Med. 9 (1998) 53–60.
[21] A.F.L. Almeida, P.B.A. Fechine, J.M. Sasaki, A.P. Ayala, J.C. Góes, D.L. Pontes, W. Margulis, A.S.B. Sombra, Optical and electrical properties of barium titanate-hydroxyapatite composite screen-printed thick films, Solid State Sci. 6 (2004) 267–278.
[22] J.C. M'Peko, J.S.C. Francis, R. Raj, Field-assisted sintering of undoped $BaTiO_3$: microstructure evolution and dielectric permittivity, J. Eur. Ceram. Soc. 34 (2014) 3655–3660.
[23] P. Gittings, C.R. Bowen, I.G. Turner, F. Baxter, J. Chaudhuri, Characterisation of ferroelectric-calcium phosphate composites and ceramics, J. Eur. Ceram. Soc. 27 (2007) 4187–4190.
[24] H. Avila, M. Reboredo, R. Parra, M. Castro, Dielectric permittivity calculation of composites based on electrospun barium titanate fibers, Mater. Res. Express 2 (2015) 045302.
[25] Y. Zhang, L. Chen, J. Zeng, K. Zhou, D. Zhang, Aligned porous barium titanate/hydroxyapatite composites with high piezoelectric coefficients for bone tissue engineering, Mater. Sci. Eng. C. 39 (2014) 143–149.
[26] A.A. Marino, J. Rosson, E. Gonzalez, L. Jones, S. Rogers, E. Fukada, Quasi-static charge interactions in bone, J. Electrost. 21 (2–3) (1988) 347–360.
[27] J.A. Spadaro, Simple biogalvanic current sources for growth control, Bioelectrochem. Bioenerg. 1 (1974) 266–274.
[28] Z. Li, Y. Qu, X. Zhang, B. Yang, Bioactive nano-titania ceramics with biomechanical compatibility prepared by doping with piezoelectric $BaTiO_3$, Acta Biomater. 5 (2009) 2189–2195.